NEURODEVELOPMENT

Mitochondrial dynamics in postmitotic cells regulate neurogenesis

Ryohei Iwata[1,2,3,4,5], Pierre Casimir[1,2,3,4,5], Pierre Vanderhaeghen[1,2,3,4,5]*

The conversion of neural stem cells into neurons is associated with the remodeling of organelles, but whether and how this is causally linked to fate change is poorly understood. We examined and manipulated mitochondrial dynamics during mouse and human cortical neurogenesis. We reveal that shortly after cortical stem cells have divided, daughter cells destined to self-renew undergo mitochondrial fusion, whereas those that retain high levels of mitochondria fission become neurons. Increased mitochondria fission promotes neuronal fate, whereas induction of mitochondria fusion after mitosis redirects daughter cells toward self-renewal. This occurs during a restricted time window that is doubled in human cells, in line with their increased self-renewal capacity. Our data reveal a postmitotic period of fate plasticity in which mitochondrial dynamics are linked with cell fate.

With neurogenesis, neural stem cells (NSCs) stop self-renewing and differentiate into postmitotic neurons. Mitochondrial dynamics, through fusion and fission, is associated with fate changes in various types of cells, including the conversion of NSCs into intermediate neural progenitors (*1*–*6*). We investigated whether and how mitochondria remodeling is coupled with neuronal fate commitment.

To examine mitochondrial dynamics during neurogenesis, we labeled mitochondria in radial glia cells (RGCs), the NSCs of the mouse embryonic cortex, through transduction of mito-GFP (green fluorescent protein fused to mitochondrial targeting sequence of COX8A) (*7*). $Pax6^+$ RGC displayed fused mitochondria, and T-box brain protein 2 $(Tbr2)^+$ intermediate neural progenitors displayed intermediate mitochondrial size (fig. S1A), as reported (*3*). Surprisingly, early-born βIII-tubulin $(βIII\text{-}tub)^+$ neurons' mitochondria were highly fragmented (Fig. 1A and fig. S1A), which was confirmed by means of immunostaining against endogenous translocase of the outer mitochondrial membrane 20 (TOMM20) (fig. S1C). Mitochondria remained fragmented for several days before gradually fusing in more mature neurons (fig. S1B).

On the other hand, mitochondria of RGCs during mitosis were fragmented (fig. S1D), which is typical of mitotic cells (*8*). We hypothesized that mitochondrial dynamics change in the daughter cells right after mitosis, depending on their prospective fate. We assessed mitochondrial dynamics of cortical progenitors through neurogenesis, from cell division to fate acquisition (Fig. 1B). We expressed in cortical progenitors the mitochondrial label mito-mNep2 (mNeptune2 protein fused to mitochondrial targeting sequence of COX8A), together with the photactivatable fluorescent protein mEOS4b (*9*), which can be photoconverted from green to red, fused to histone protein H2B to target chromatin (H2B-mEOS4b). This enabled the identification of cells in mitotic metaphase/anaphase, based on labeling of chromatin with fluorescent mEOS proteins. Such cells were tagged by means of photoconversion, enabling the tracking of the daughter cells and their mitochondria 1 to 24 hours after mitosis. We used expression of βIII-tub as a neuronal marker and Tbr2 for intermediate neural progenitors. Cells that expressed neither Tbr2 nor βIII-tub corresponded mostly (95%) to $Sox2^+$ RGC (fig. S1E). The acquisition and stabilization of the identity of daughter cells could then be observed over the next 6 to 12 hours (fig. S1F), with similar timing as that reported in vivo (*10*). Mitochondrial dynamics in the first 3 hours after cell division were characterized either by increased mitochondrial length or by retaining shorter fragmented mitochondria (Fig. 1C). Presumptive RGC displayed long mitochondria, presumptive neurons retained short mitochondria, and intermediate progenitors displayed intermediate-sized mitochondria (Fig. 1C).

Could postmitotic alteration of mitochondrial dynamics influence neurogenesis? We tracked postmitotic cells, this time using compounds that promote mitochondria fusion [M1, (E)-4-chloro-2-(1-(2-(2,4,6-trichlorophenyl) hydrazono)ethyl)phenol (*11*)] or inhibit mitochondria fission [mitochondrial division inhibitor (Mdivi-1), 3-(2,4-dichloro-5-methoxyphenyl)-2-sulfanyl-4(3H)-quinazolinone (*12*)]. Compounds were added to the photoconverted cells right after mitosis (Fig. 1D), which resulted in an increase of mitochondrial size within 3 hours of postmitotic cell labeling (Fig. 1E). The identity of daughter cells was not significantly altered at 3 hours after treatment (Fig. 1F) but changed by 6 hours after treatment: The proportion of daughter cells that became RGCs increased, and the proportion that became neurons decreased, whereas the proportion of intermediate progenitors remained unchanged (Fig. 1, G and H). The number of cells was unchanged in either condition, excluding cell loss as a cause (fig. S2, A and B). The effect of M1 treatment on cell fate was maintained at 12 hours, with an increase in non-neurogenic divisions at the expense of neurogenic divisions (fig. S2, C and D), resulting in an increase in clonal size at 24 hours (fig. S2, E to G), indicating that RGCs generated under M1 treatment stably retained their self-renewal capacity. Morphogenesis of the neurons that could still be generated under M1 treatment also appeared to be normal at 24 hours (fig. S2H). To explore upstream mechanisms, we examined Drp1 that is activated during mitosis through CDK1 phosphorylation (*13*). We found high levels of pDrp1 in mitotic cells, followed by a dual pattern of phosphorylation, inversely correlated with mitochondrial size (fig. S3A). Postmitotic treatment with Roscovitine, an inhibitor of CDK activity, led to increased size of mitochondria, fewer neurons, and more RGCs, with no detectable cell loss (fig. S3, B to E).

Thus, in vitro with chemical intervention, increased fusion or decreased fission of mitochondria after mother RGC division biases fate acquisition of the daughter cells in favor of stem cell fate at the expense of neuronal fate. We next examined in vivo mouse corticogenesis with genetic manipulation of mitochondrial dynamics. We suppressed the expression of Drp1 by means of in utero electroporation and observed a decrease in the proportion of generated neurons and an increase in the proportion of intermediate progenitors and RGCs (Fig. 2, A and B). To test postmitotic manipulation of mitochondrial dynamics in vivo, we used the FlashTag method that enables in utero labeling of RGCs during mitosis (*10*). Injection of FlashTag, together with M1 to promote mitochondria fusion, resulted in increased mitochondria size within 4 hours (Fig. 2C). $FlashTag^+$-labeled cells 12 hours after M1 or Mdivi-1 treatment revealed an increase in the proportion of $Sox2^+$ RGCs and $Tbr2^+$ intermediate progenitors and a decrease of $Neurod2^+$ neurons (Fig. 2D). Thus, mitochondrial dynamics after mitosis affect mouse cortical neurogenesis in vivo, like in vitro.

We sought to examine whether the mitochondrial oxidation state could mediate these effects (*3*, *14*) by testing the ionophore carbonyl cyanide *m*-chlorophenyl hydrazone (CCCP), which leads to hyperactivation of the electron transport chain, and thereby increased reactive oxygen species and oxidized nicotinamide

[1]VIB Center for Brain and Disease Research, 3000 Leuven, Belgium. [2]Department of Neurosciences, Katholieke Universiteit (KU) Leuven, 3000 Leuven, Belgium. [3]Leuven Brain Institute, KU Leuven, 3000 Leuven, Belgium. [4]Institut de Recherches en Biologie Humaine et Moléculaire (IRIBHM), Université Libre de Bruxelles (ULB), 1070 Brussels, Belgium. [5]ULB Neuroscience Institute (UNI), ULB, 1070 Brussels, Belgium.
*Corresponding author. Email: pierre.vanderhaeghen@kuleuven.vib.be

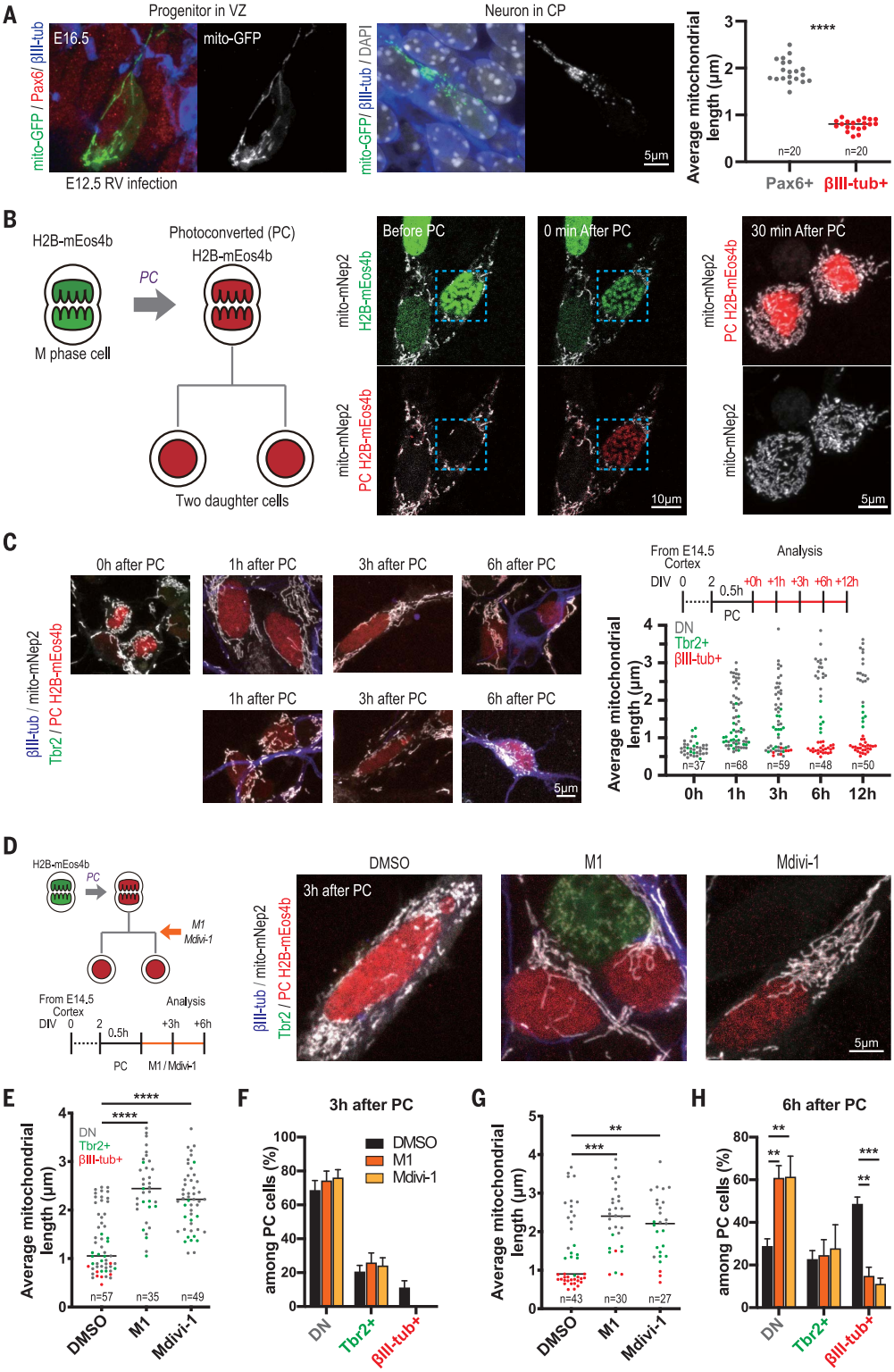

Fig. 1. Mitochondrial dynamics influence fate decision in postmitotic cortical cells. (**A**) Representative images of mitochondrial morphology (mito-GFP) in Pax6$^+$ RGCs in (left) ventricular zone (VZ) and (middle) βIII-tub$^+$ newborn neuron in cortical plate (CP) in embryonic day 16.5 (E16.5) mouse cortex, after in utero retroviral infection at E12.5. (Right) Quantified mitochondrial length from two biological replicate experiments. Each data point represents an individual cell average mitochondrial size. ****P < 0.0001; unpaired Student's t test. (**B**) (Left) Schematic of the labeling strategy by using photoconverted (PC) histone H2B-mEos4b. (Right) Representative images of PC cell labeled with mito-Nep2. (**C**) (Left) Representative images and timeline of PC experiment to determine kinetics of mitochondrial dynamics after mitosis in mouse embryonic cortical cells. (Right) Quantified mitochondrial length from three biological replicate experiments. Each data point represents an individual cell average mitochondrial size, together with fate marker expression. Red, βIII-tub$^+$ neuron; green, Tbr2$^+$ intermediate progenitor; gray, double negative (DN) RGC. (**D**) Timeline and representative images of PC experiment by using M1 and Mdivi-1. DMSO, dimethyl sulfoxide. (**E** and **G**) Quantified mitochondrial length from three biological replicate experiments. (E) Three hours after label. (G) Six hours after PC. Each data point represents an individual cell average mitochondrial size. **P < 0.01, ***P < 0.001, ****P ≤ 0.0001; Dunnett's multiple comparisons test. (**F** and **H**) Quantification of each cell fate marker$^+$ cells among PC cells from at least four biological replicate experiments. Data are shown as mean ± SEM. **P < 0.01, ***P < 0.001; Dunn's multiple comparisons test.

adenine dinucleotide (NAD$^+$)/reduced NAD$^+$ (NADH) ratio (*15*). This resulted in increased neurogenesis within 6 hours after mitosis, without change in mitochondria size (Fig. 3, A and B, and fig. S4A). We next tested the implication of Sirtuin-1 (Sirt1), which is activated by increased NAD$^+$/NADH ratio (*16*) and promotes cortical neurogenesis together with the BCL6 transcriptional repressor (*17*, *18*). We found that Sirt1 inhibition through Ex-527 treatment in postmitotic cells blocked neurogenesis, also after CCCP treatment (Fig. 3C and fig. S4, B to D). Sirt1 promotes neurogenesis through H4K16 histone deacetylation at BCL6 transcriptional targets (*17*, *19*). We therefore examined H4K16 acetylation levels, which we found to be increased after Ex-527 treatment and decreased after CCCP treatment (Fig. 3D). We next

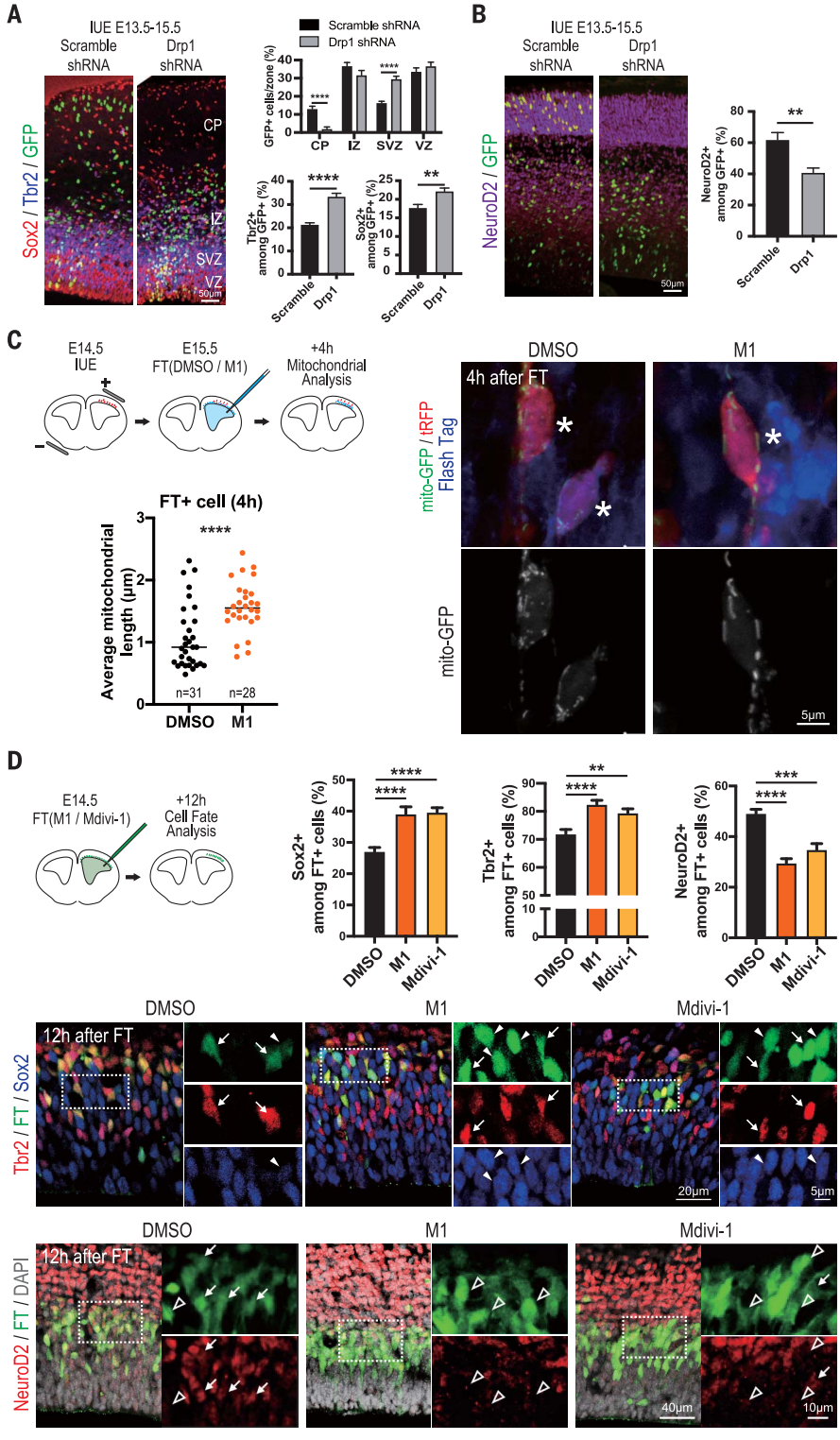

Fig. 2. Mitochondrial dynamics in post-mitotic cells affect cortical neurogenesis in vivo. (**A** and **B**) (Left) In utero electroporation (IUE) of scramble or Drp1 short hairpin RNA (shRNA) at E13.5, analyzed at E15.5. Histogram shows the percentage of H2B-GFP$^+$ cells in VZ, SVZ, IZ, and CP. (Right) Quantification of (A) Tbr2$^+$ or Sox2$^+$ and (B) NeuroD2$^+$ cells among electroporated cells from two biological replicate experiments. Data are shown as mean ± SEM. $^{**}P < 0.01$, $^{****}P < 0.0001$; [(A), top] Bonferroni's multiple comparisons test, [(A), bottom] unpaired *t* test, (B) Mann-Whitney test. (**C**) (Top left) Timeline of in utero electroporation [Turbo red fluorescent protein (tRFP) and mito-GFP] and FlashTag (FT) labeling. (Right) Representative images of M1-treated tRFP and mito-GFP electroporated FT$^+$ cell (asterisks). (Bottom left) Quantification of mitochondrial length from two biological replicate experiments. Each data point represents an individual cell average mitochondrial size. $^{****}P < 0.0001$; Mann-Whitney test. (**D**) (Left) Schematic and representative images of in utero M1 treatment and FT labeling in the mouse embryonic cortex. (Right) Quantification of Sox2$^+$, Tbr2$^+$, and NeuroD2$^+$ cells among FT$^+$ cells from two biological replicate experiments. Data are shown as mean ± SEM. $^{**}P < 0.01$, $^{***}P < 0.001$, $^{****}P < 0.0001$; Sox2 and Tbr2, Dunn's multiple comparisons test; NeuroD2, Dunn's multiple comparisons test. (Top) Arrows indicate Sox2$^+$, and arrowheads indicate Tbr2$^+$. (Bottom) Arrows indicate NeuroD2$^+$, and open arrowheads indicate NeuroD2$^-$.

explored potential links between mitochondrial dynamics and Sirtuins. We found that Sirtuin activation under SRT1720 treatment could abolish the effects of M1 on neurogenesis (fig. S4, E to G) and that H4K16 acetylation was increased after M1 or Mdivi-1 treatment (Fig. 3D). These data suggest that mitochondrial influence on neurogenesis may involve, at least in part, Sirt1.

Human cortical progenitors are characterized by intrinsic higher self-renewal potential that is thought to underlie the evolutionary increase in human cortical size (*20*, *21*). We examined mitochondrial dynamics during in vitro corticogenesis from human pluripotent stem cells. As in the mouse, human cortical RGCs were characterized by large mitochondria, whereas early-born neurons displayed fragmented mitochondria (Fig. 4A). Overexpression of mitochondrial fission–promoting Drp1 or mitochondrial fission factor (MFF) genes in

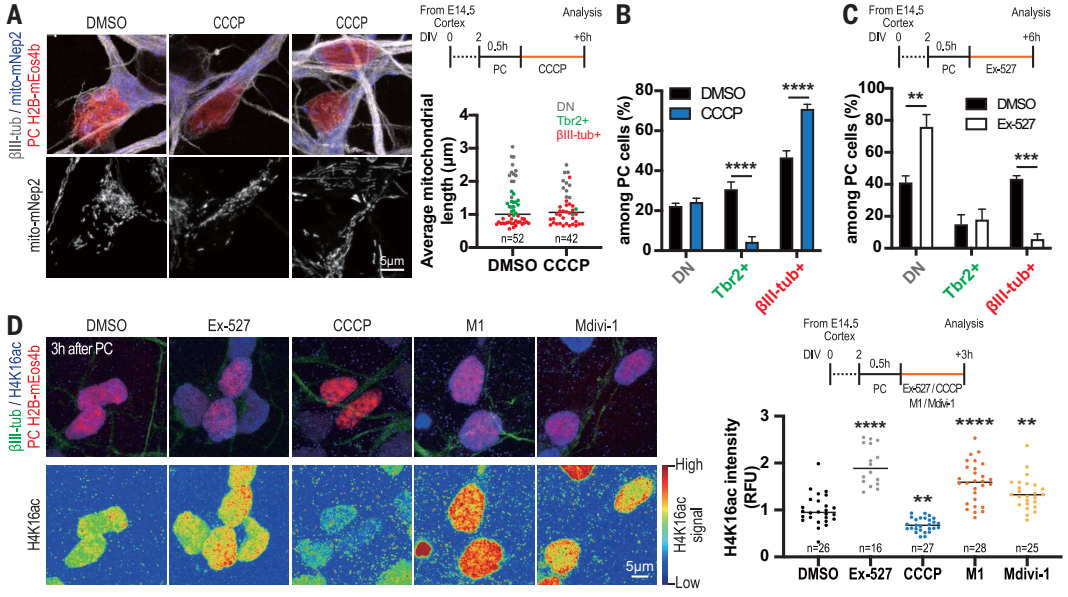

Fig. 3. Mitochondria and Sirtuin activity influence cortical neurogenesis. (**A**) Timeline, representative images, and quantified mitochondrial length after CCCP postmitotic treatment. Each data point represents an individual cell average mitochondrial size from three biological replicate experiments. Mann-Whitney test. (**B**) Quantification of each cell fate marker$^+$ cells among PC cells (6 hours after label) from three biological replicate experiments after CCCP postmitotic treatment. Data are shown as mean ± SEM. $^{****}P < 0.0001$; Bonferroni's multiple comparisons test. (**C**) Timeline and quantification of PC cells expressing cell fate markers by using Sirt1 inhibitor Ex-527 from three biological replicate experiments. Data are shown as mean ± SEM. $^{**}P < 0.01$, $^{***}P < 0.001$; Bonferroni's multiple comparisons test. (**D**) (Top right) Timeline and (left) representative images of H4K16ac signal in PC cells. (Bottom right) Quantified H4K16ac signal from two biological replicate experiments. Each data point represents an individual cell average H4K16ac signal. $^{**}P < 0.01$, $^{****}P < 0.0001$; Dunn's multiple comparisons test.

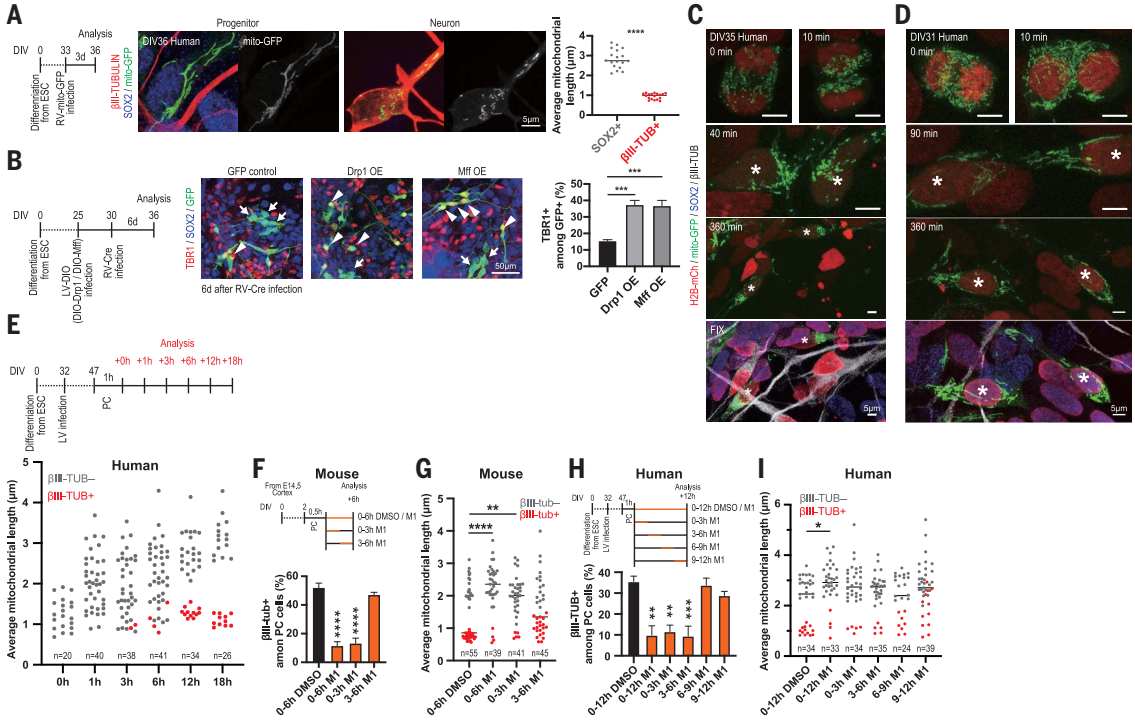

Fig. 4. A species-specific postmitotic period of fate plasticity. (**A**) (Left and middle) Timeline and representative images of mitochondrial morphology in SOX2$^+$ (RGC) and βIII-tub$^+$ (Newborn neuron) human embryonic stem cell (ESC)–derived cortical cell 3 days after mito-GFP retroviral infection. (Right) Quantification of mitochondrial length from two biological replicate experiments. Each data point represents an individual cell average mitochondrial size. $^{****}P < 0.0001$; Mann-Whitney test. (**B**) (Left and middle) Timeline and representative images of Drp1- and Mff-overexpressing human cortical cells (6 days after Cre-expressing retrovirus infection). Arrowheads indicate Neuron (Tbr1$^+$), and arrows indicate Progenitor (Sox2$^+$). (Right) Quantification of TBR1$^+$ cells among GFP-labeled cells from three biological replicate experiments. Data are shown as mean ± SEM. $^{***}P < 0.001$; Dunnett's multiple comparisons test. (**C** and **D**) Representative time-lapse images of mitochondrial dynamics in (C) neurogenic division and (D) non-neurogenic division. Asterisks indicate tracked cells. (**E**) (Top) Timeline of photoconversion experiment and (bottom) quantified mitochondrial length from three biological replicate experiments. Each data point represents an individual cell average mitochondrial size. (**F** and **H**) (Top) Timeline of M1 treatment in (F) mouse and (H) human cortical cells. (Bottom) Quantification of βIII-tub$^+$ cells among PC cells from three biological replicate experiments. Data are shown as mean ± SEM. $^{**}P < 0.01$, $^{***}P < 0.001$, $^{****}P < 0.0001$; Dunnett's multiple comparisons test. (**G** and **I**) Quantification of mitochondrial length in (G) mouse and (I) human cortical cells from three biological replicate experiments. Each data point represents an individual cell average mitochondrial size. $^{*}P < 0.05$, $^{**}P < 0.01$, $^{****}P < 0.0001$; Dunn's multiple comparisons test.

human RGCs resulted in increased neurogenesis (Fig, 4B).

We next performed time-lapse imaging of human cortical progenitors labeled with mito-GFP, followed by fate marker determination (Fig. 4, C and D). This revealed that at mitosis, the mitochondria were fragmented. After mitosis, as for mouse cells, human cells with large mitochondria remain progenitors, whereas those with fragmented mitochondria become neurons (n = 24 cells). Similar data were obtained by using mEOS labeling of human mitotic RGC, like in the mouse (Fig. 4E and fig. S5A). M1 treatment after mitosis of human progenitors led to increased mitochondria size and decreased neuronal differentiation, as well as increased self-renewing division (Fig. 4I and fig. S5, B and C).

Thus, postmitotic control of cell fates through mitochondrial dynamics is conserved in mouse and human corticogenesis. We next used the mEOS system to determine the length of the susceptibility phase during which mitochondrial dynamics can affect neural cell fate. We speculated that given the higher self-renewal potential of human RGCs, the susceptiblity phase might be longer in these cells. Human and mouse cells were treated in parallel over defined time periods after mitosis (Fig. 4, F to I). In the mouse, M1 treatment altered cell fate up to but not beyond 3 hours after mitosis (Fig. 4F). In human cells, M1 treatment altered cell fate up to 6 hours after mitosis (Fig. 4H), indicating that the susceptibility phase of postmitotic neural cell fate plasticity is doubled compared with mouse cells.

Our data suggest important mitochondria remodeling during postmitotic phases of neurogenesis, which will have to be characterized further with electron microscopy and metabolic analyses. Previous data emphasized fate decision of NSCs before mitosis (*22*–*24*). Our data reveal a fate plasticity period that extends much later, shortly after NSC mitosis. This period is longer in human than in mouse cortical progenitors, which could contribute to their increased self-renewal capacities (*20*, *21*). High levels of mitochondria fission in newborn neurons themselves lead to irreversible fate commitment, in link with developmental neurogenic pathways, through mechanisms that remain to be elucidated.

REFERENCES AND NOTES

1. K. Mitra, R. Rikhy, M. Lilly, J. Lippincott-Schwartz, *J. Cell Biol.* **197**, 487–497 (2012).
2. M. D. D. Buck *et al*., *Cell* **166**, 63–76 (2016).
3. M. Khacho *et al*., *Cell Stem Cell* **19**, 232–247 (2016).
4. A. Kasahara, S. Cipolat, Y. Chen, G. W. Dorn 2nd, L. Scorrano, *Science* **342**, 734–737 (2013).
5. A. Bahat, A. Gross, *J. Biol. Chem.* **294**, 13852–13863 (2019).
6. L. Pernas, L. Scorrano, *Annu. Rev. Physiol.* **78**, 505–531 (2016).
7. R. Rizzuto, M. Brini, P. Pizzo, M. Murgia, T. Pozzan, *Curr. Biol.* **5**, 635–642 (1995).
8. P. Mishra, D. C. Chan, *Nat. Rev. Mol. Cell Biol.* **15**, 634–646 (2014).
9. M. G. Paez-Segala *et al*., *Nat. Methods* **12**, 215–218, 4, 218 (2015).
10. L. Telley *et al*., *Science* **351**, 1443–1446 (2016).
11. D. Wang *et al*., *Angew. Chem. Int. Ed.* **51**, 9302–9305 (2012).
12. A. Cassidy-Stone *et al*., *Dev. Cell* **14**, 193–204 (2008).
13. N. Taguchi, N. Ishihara, A. Jofuku, T. Oka, K. Mihara, *J. Biol. Chem.* **282**, 11521–11529 (2007).
14. M. Liesa, O. S. Shirihai, *Cell Metab.* **17**, 491–506 (2013).
15. X. R. Bao *et al*., *eLife* **5**, e10575 (2016).
16. C. Cantó, K. J. Menzies, J. Auwerx, *Cell Metab.* **22**, 31–53 (2015).
17. L. Tiberi *et al*., *Nat. Neurosci.* **15**, 1627–1635 (2012).
18. S. Hisahara *et al*., *Proc. Natl. Acad. Sci. U.S.A.* **105**, 15599–15604 (2008).
19. J. Bonnefont *et al*., *Neuron* **103**, 1096–1108.e4 (2019).
20. I. K. I. K. Suzuki *et al*., *Cell* **173**, 1370–1384.e16 (2018).
21. I. Espuny-Camacho *et al*., *Neuron* **77**, 440–456 (2013).
22. C. Dehay, H. Kennedy, *Nat. Rev. Neurosci.* **8**, 438–450 (2007).
23. P. Salomoni, F. Calegari, *Trends Cell Biol.* **20**, 233–243 (2010).
24. T. Edlund, T. M. Jessell, *Cell* **96**, 211–224 (1999).

ACKNOWLEDGMENTS

We thank members of the laboratory and CBD for helpful discussions and the ULB Light Microscopy Facility for support with imaging. **Funding:** This work was funded by Grants of the European Research Council (GENDEVOCORTEX), the Belgian FWO and FRS/FNRS, the AXA Research Fund, the Belgian Queen Elizabeth Foundation, and the Fondation ULB (to P.V.). Some of the images were acquired on a Zeiss LSM 880 system supported by Hercules AKUL/15/37_GOH1816N and FWO G.0929.15 to P. Vanden Berghe, KU Leuven. R.I. was supported by a postdoctoral fellowship of the FRS/FNRS, and P.C. holds a Ph.D. fellowship of the FWO (file number 51989). **Author contributions:** Conceptualization and methodology, R.I. and P.V.; investigation, R.I., P.C., and P.V.; formal analysis, R.I., P.C., and P.V.; writing, R.I. and P.V; funding acquisition, P.V.; resources, P.V.; supervision, P.V. **Competing interests:** The authors declare no competing interests. **Data and materials availability:** All data are available in the manuscript or the supplementary materials. All materials are available upon request from P.V.

SUPPLEMENTARY MATERIALS

science.sciencemag.org/content/369/6505/858/suppl/DC1
Materials and Methods
Figs. S1 to S5
Reference (*25*)
MDAR Reproducibility Checklist

View/request a protocol for this paper from *Bio-protocol*.

7 February 2020; accepted 22 June 2020
10.1126/science.aba9760

Science

Mitochondrial dynamics in postmitotic cells regulate neurogenesis

Ryohei Iwata, Pierre Casimir and Pierre Vanderhaeghen

Science **369** (6505), 858-862.
DOI: 10.1126/science.aba9760

Mitochondrial dynamics and cell fate

Radial glia cells, the stem cells of early brain development, can generate more of themselves or generate differentiating neurons. Iwata *et al.* now show that these fate decisions involve the mitochondria. Cells that have fragmented mitochondria shortly after mitosis are more likely to become neurons, whereas cells that are undergoing mitochondrial fusion are likely to continue being stem cells.

Science, this issue p. 858